

## Model optimization and economic analysis of a multi-effect diffusion solar distiller

Byung-Ju Lim (Ph.D.)<sup>a</sup>, Ga-Ram Lee (Master)<sup>a,b</sup>, Seok-Min Choi (Ph.D.)<sup>a</sup>,  
Kyung-Yul Chung (Ph.D.)<sup>a</sup>, Chang-Dae Park (Ph.D.)<sup>a,b,\*,\*</sup>

<sup>a</sup> Energy Systems Research Division, Korea Institute of Machinery & Materials, 156 Gajeongbuk-Ro, Yuseong-Gu, Daejeon 34103, Republic of Korea

<sup>b</sup> Department of Plant system and Machinery, University of Science & Technology, 217 Gajeong-Ro, Yuseong-Gu, Daejeon 34113, Republic of Korea

### ARTICLE INFO

#### Keywords:

Vertical multi-effect diffusion solar distiller  
Optimization  
Numerical analysis  
Economic analysis  
Small capacity

### ABSTRACT

This study focused on finding the maximum productivity by optimizing vertical multi-effect diffusion solar distiller (VMED) and lowering the water cost of that. The numerical model of the VMED was experimentally validated, and then used to find the optimal conditions for the essential variables. The VMED consists of a glass cover, plates, wicks, and a seawater feeding unit. Each effect has a cotton-cloth wick attached to one side of the plate. This VMED repeatedly using condensation latent heat can get more production than that of conventional solar still. The numerical result showed that the optimum values of the gap distance of double glass cover and the number of effects were 25–30 mm and 10–15, and the feed flow rates of spring, summer, fall, and winter were optimal in 9, 16, 10, and 3 g/min, respectively in supplying same flow rate into all the effects. The maximum productions for all seasons (spring, summer, fall, and winter) were 16.6, 36.0, 19.0, 2.5 kg/(m<sup>2</sup>·d), respectively in South Korea. Economic analysis showed that the potential water price of the VMED was 6.1 \$/m<sup>3</sup>, which was more competitive in the market than other solar desalination systems with a small capacity of < 100 m<sup>3</sup>/d.

### 1. Introduction

The world population has encountered a scarcity of fresh water due to a global imbalance between supply and demand for fresh water for a long time. And the population increase, industrialization, civilization, and global warming have aggravated the global water problem. It is assumed that > 70% of the world population will encounter a water shortage problem by 2025 [1–3]. To overcome the problem, desalination technology might have been more relatively economical and reliable than traditional water supply methods, and the utilization continued to increase [4]. Notably, solar desalination can be an eco-friendly and cost-effective technique to get fresh water as purifying saline water.

The solar still is a well-known type of solar desalination system due to simplicity in construction and operation, and low production cost [5,6]. However, the daily production of conventional solar stills (CSS) as a representative model of solar stills is small as < 5 kg/(m<sup>2</sup>·d) [7]. Many researchers have studied various advanced solar stills to enhance their productions. Of those advanced solar stills, a multi-effect distillation has attracted attention due to repeatedly using condensation

latent heat and hence the dramatic increase in the water production [8].

Many studies have been conducted on a vertical multi-effect diffusion solar distiller (VMED) which consists of multiple plates vertically arranged at a narrow interval for repeatedly using incident solar energy and latent heat. In 1964, Kudret Selçuk [9] developed a 2-effect VMED with double cover glass and evaporation-condensation plates. This VMED had many troughs which were installed on one side of the plate and used as the evaporation surface. When the seawater was supplied to the troughs, the water level gradually rose and was no longer increased by the tube installed in the trough, and the seawater flowed along the tube down and was supplied to the trough below. Since the troughs were installed continuously in a vertical direction on the plate, the seawater supplied from the top of a plate filled all the troughs. Solar energy penetrated the glass cover of this VMED and was absorbed by the black plate to heat the seawater supplied to the rear side. The heated seawater was diffused after evaporation and condensed on the plates of the next effect, where the latent heat of condensation was transferred to the plates. After all, the production efficiency of the VMED increased due to this twice repeated evaporation-condensation

\* Corresponding author at: Energy Systems Research Division, Korea Institute of Machinery & Materials, 156 Gajeongbuk-Ro, Yuseong-Gu, Daejeon 34103, Republic of Korea.

E-mail addresses: [bzoo77@kimm.re.kr](mailto:bzoo77@kimm.re.kr) (B.-J. Lim), [ccl3455@kimm.re.kr](mailto:ccl3455@kimm.re.kr) (G.-R. Lee), [choism@kimm.re.kr](mailto:choism@kimm.re.kr) (S.-M. Choi), [kychung@kimm.re.kr](mailto:kychung@kimm.re.kr) (K.-Y. Chung), [parkcdae@kimm.re.kr](mailto:parkcdae@kimm.re.kr) (C.-D. Park).

<https://doi.org/10.1016/j.desal.2020.114446>

Received 7 February 2020; Received in revised form 23 March 2020; Accepted 23 March 2020

Available online 22 April 2020

0011-9164/ © 2020 Elsevier B.V. All rights reserved.

**Nomenclature**

$A$	Area, $m^2$
$c$	Specific heat, $J/(kg\ K)$
$D$	Diffusivity of vapor, $m^2/s$
$DR$	Decreasing rate of feed flow rate to next effect, %
$d$	Distance or diffusion gap, m
$G$	Solar irradiance, $W/m^2$
$h_a$	Convective heat transfer coefficient, $W/(m^2\ K)$
$k$	Thermal conductivity, $W/(m\ K)$
$M$	Annual fresh water total production, $kg/yr$
$\dot{m}$	Mass flow rate, $kg/s$
$\dot{m}_e$	Evaporative mass flow rate, $kg/s$
$\dot{m}_f$	Feed flow rate of seawater, $g/min$
$m_t$	Daily total production, kg
$Nu$	Nusselt number
$N_t$	Total numbers of effects
$P$	Total pressure, Pa
$p$	Partial pressure of saturated vapor, Pa
$\dot{Q}$	Heat flow rate, W
$Ra$	Rayleigh number
$R_v$	Specific gas constant of water vapor, $J/(kg\ K)$
$T_m$	Average temperature, K
$t$	Time, s

**Subscript**

atm:	Ambient
c:	Convection
cd:	Cold part
d:	Conduction
df:	Diffuse radiation
dr:	Direct radiation
g:	Glass
gi:	Inner glass
go:	Outer glass
glb:	Global
ht:	Hot part
in:	Inlet

min:	Minimum
n:	Horizontal surface
r:	Radiation
slr:	Solar energy
w:	Wick
v:	Vapor

**Greek**

$\alpha$ :	Solar altitude angle, $^\circ$
$\beta$ :	Tiled angle of distiller, $^\circ$
$\theta$ :	Solar incident angle, $^\circ$
$\eta$ :	Absorptance
$\varepsilon$ :	Emittance
$\rho$ :	Density, $kg/m^3$
$\xi$ :	Azimuth angle, $^\circ$
$\tau$ :	Transmittance

**Abbreviations**

ASV	Annual salvage value
AC	Annual cost
AMC	Annual maintenance operational cost
CSS	Conventional solar still
CRF	Capital recovery factor
CPT	Cost of distilled water per ton
FAC	Fixed annual cost
HMED	Hybrid multi-effect solar distiller
MD	Membrane distillation
MED	Multi-effect solar distiller
MSF	Multi-stage flash
SFF	Sinking fund factor
PC	Present capital cost
PV	Photovoltaic
RO	Reverse osmosis
SV	Salvage value
VMED	Vertical multi-effect solar distiller

process. Cooper and Appleyard [10] developed a 3-effect VMED. They used a cloth wick instead of troughs to increase the evaporation area of the seawater on the plate. The experimental results showed that the VMED productivity increased over that of CSS. Elsayed et al. [11] found that freshwater production increased as a decrease of seawater feed rate through an experimental study on 3-effect VMED. Ouahes et al. [12] obtained  $15\ kg/(m^2\cdot d)$  of fresh water through the experiment of 3-effect VMED, and the production of CSS was  $2.5\text{--}3\ kg/(m^2\cdot d)$  under the same conditions. Ohshiro et al. [13] and Tanaka et al. [14] found that the VMED increased water production as the diffusion interval of the effects decreased. Nosoko et al. [15] conducted a theoretical study on the performance characteristics of 10-effect VMED. This VMED was operated by the thermal energy of steam, and was intended to increase efficiency by recovering thermal energy of concentrated seawater discharged from the effects. They numerically obtained a vertical distribution of temperature and concentration of seawater in the wick. Besides, they found that the concentration of the seawater flowing down along the wick gradually increased due to evaporation and the boiling point of the seawater rose, and then production decreased. Tanaka [16] developed the VMED using the thermal energy of biomass burned in a stove. The experimental results showed that the water production of the still was about 0.75 and 1.35 kg during the first 2 h of burning from a single-effect and 4-effects VMEDs, respectively. Park et al. [17–19] developed a single-effect VMED that reused the exhaust

gas thermal energy of an electric generator which mainly used in islands and remote areas. Moreover, the experimental results showed that the VMED obtained 6.7 kg of fresh water at 0.83 kW of thermal energy for 3 h. They assumed that the production could increase by at least 19.4 kg/d for ten-effect VMED. Xie et al. [20] developed the VMED with vertical ripple surface and solar collector. They pointed out the problem of wick's peeling-off from the plate on long-term usage and replaced the wick into troughs for better reliability and a more compact structure. Developed 3-effect VMED produced fresh water of  $10.3\ kg/(m^2\cdot d)$  at  $26.1\ MJ/(m^2\cdot d)$  numerically and  $5.74\ kg/(m^2\cdot d)$  at  $22.77\ MJ/(m^2\cdot d)$  experimentally. Reddy and Sharon [21] numerically studied on active VMED with a vacuum pump. The analysis results showed that the 3-effect VMED produced the maximum annual average distillate of  $21.29\ kg/(m^2\cdot d)$  under the low pressure operation of 0.25 bar and the water cost of the VMED was about 0.019 \$/kg.

In order to improve the performance of the VMED, many researches have been conducted on modified VMED with new structures and equipment. Some researchers [22–27] studied on a hybrid multi-effect solar distiller (HMED) which integrated with the VMED and the CSS. They studied to find the performance characteristics and the optimal parameters by numerical analysis and performance test. Tanaka et al. [22] got fresh water of  $14.8\text{--}18.7\ kg/(m^2\cdot d)$  at  $20.9\text{--}22.4\ MJ/(m^2\cdot d)$  solar insolation to glass cover of CSS section from the 10-effect HMED. Tanaka et al. [23] theoretically obtained that the productivity of the 13-

effect HMED with 5 mm effect gaps was four times more than the CSS and increasing the saline water feed rates to the wicks of VMED section and initial saline water level of the CSS section decreased production of the HMED. Yeo et al. [24] conducted an experimental study to investigate the performance characteristics of different heat sources such as solar heat, electric heater, and waste heat in 10-effect HMED. Experimental results showed that fresh water was simultaneously obtained from CSS and VMED section in HMED, but the fresh water production ratio of the VMED section was up to 16 times higher. They suggested that the optimum ratio of the feed flow rate of seawater to evaporation rate in the MED section may be within a range of 4.6–2.8, regardless of heat sources. Park et al. [25,26] conducted the performance characteristics experiment using waste heat as the heat source for the 1-effect and 10-effect HMED. Experimental results showed that the 1-effect and 10-effect HMED produced distilled water of 17.1–19.6 kg/(m<sup>2</sup>·d) at 3000 kJ/h of heat flow rate and 18.02 kg/(m<sup>2</sup>·d) at 22.37 MJ of total heat input, respectively. Kaushal et al. [27] developed the HMED with a floating wick on basin seawater. The test results showed that the HMED produced the fresh water of 9.89 kg/(m<sup>2</sup>·d) at 24.6 MJ/(m<sup>2</sup>·d) of a clear sunny day in April. They found that productivity of the still was 21% higher than the HMED without floating wick.

Tanaka et al. [28] studied the VMED with a reflector to increase the solar energy absorption. They found that 1-effect VMED with reflector produced 4.39 kg/(m<sup>2</sup>·d) at 16.8 MJ/(m<sup>2</sup>·d) and assumed that increasing the effect numbers to 10 would increase the production by 5–6 times. Besides, Tanaka et al. [29,30] studied the VMED with tilted wick still. Because the vapor evaporated from the wick of the tilted wick section condensates at the plate of the VMED section, the VMED can additionally get the condensation latent heat. Fresh water production of 1-effect and 9-effect VMED with tilted wick still 4.88 kg/(m<sup>2</sup>·d) in 13.6 MJ/(m<sup>2</sup>·d) [29] and 19.2 kg/(m<sup>2</sup>·d) at the spring equinox in Japan [30], respectively. Huang et al. [31] developed the 10-effect VMED with a spiral shape plate and a vacuum tube solar collector. They found that this VMED produced water of 19.7 kg/(m<sup>2</sup>·d) at 800 W/m<sup>2</sup>. Chong et al. [32] developed the 18-effect VMED with a non-metallic bended-plate and a vacuum tube solar collector. They found that this VMED produced 23.9 kg/(m<sup>2</sup>·d) at 22.1 MJ/(m<sup>2</sup>·d). Huang et al. [33] developed 6-effect VMED with concentric tubular and found that the product of that was 1.84 kg m<sup>2</sup>/h under the solar intensity of 1 kW/m<sup>2</sup>. Katsuhito Fukui et al. [34] theoretically studied on horizontal MED as a maritime lifesaver. The proposed 6-effect MED was predicted to produce about 15 kg/(m<sup>2</sup>·d) on a sunny day of 22 MJ/(m<sup>2</sup>·d) solar radiation.

From our previous study [35], the maximum production of the 10-effect VMED was 16.6 kg/m<sup>2</sup> on the summer solstice. We found the

optimal values for essential variables (feed flow rate, inclination angle, wind speed, and the number of effects) and their performance characteristics. For the operational variables of the VMED, the optimum seawater feeding flow rate was 7.3 g/min based on a plate area of 1 m<sup>2</sup>. For design variables, the distiller's production was independent of an aspect ratio of the plate at a given solar insolation area. In South Korea, an optimum inclination angle from the ground was of 40–50°. The optimal number of effects of the VMED must be selected based on the condition of the summer solstice; and the optimal number was 11. Installing the VMED in a poorly ventilated place was recommended due to the decrease in production with wind speed.

The studies on the VMEDs integrated with various equipment (CSS, electric generator, reflector, tilted wick still, vacuum pump) or applied with new effect shapes (bent type, spiral type) have also been performed to increase production efficiency. However, the VMEDs combined with the various equipment might be placed with the burden of operation and management. Moreover, the VMEDs with new shapes will have the inevitably same problems because they structurally receive thermal energy from an external heat source such as solar collectors. As the conventional VMEDs which only were constituted with the flat plates and wicks without other equipment have significant advantages on low cost, structural simplicity, and operation convenience, the researches on efficiency increase are still needed. In particular, for commercialization of the VMED, both high efficiency and low water cost are very crucial, so this VMED is necessary to be optimized on considering economic view. In many proceeding studies [23,24,35], they found the optimal conditions for each performance variable but did not present the maximum production applying synthetically on all the optimum variable. In addition, the optimization focused only on the point of view of the amount of production and did not take economic considerations into account. In order to enter the desalination market, it is necessary to compare the water cost with other solar distillers and select an application target of the appropriate production capacity.

In this study, we focused on finding the maximum productivity considering simultaneously the optimum values of all the variables and lowering the water cost of our VMED than other solar stills. We conducted a study on VMED with double glazing glass cover that could reduce heat loss to improve performance as pointed out in our previous study [35]. We analyzed the performance characteristics of essential variables such as gap distance of double glazing glass cover, the number of effects, effect plate material, feed flow rate, decreasing ratio of the feed flow rate, of this VMED. But uncontrollable environment variables such as wind speed, solar radiation, environmental temperature were not optimum variable targets of this study and the variables already discovered (gap between effects and inclined angle on the ground) from

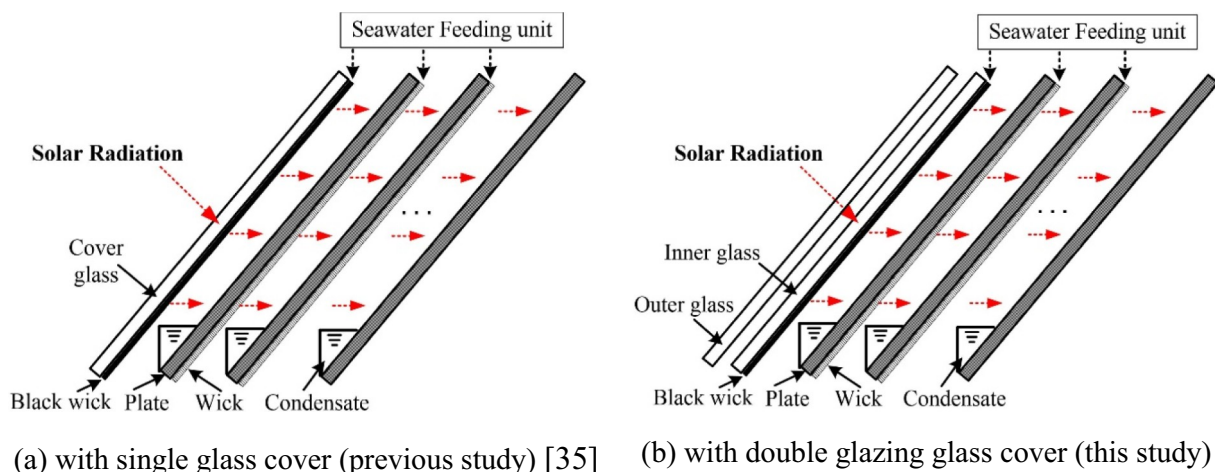


Fig. 1. Schematic diagrams of the VMED.

previous studies were applied to this study. In addition, we analyzed the water cost of the VMED to compare with other solar stills and presented the optimization method to make it more competitive considering the commercialization. In order to find a suitable capacity for a price competitiveness, we also compared and analyzed with the water costs according to the capacity of various types of solar desalination systems.

## 2. Multi-effect diffusion still with double glass cover

The schematic of the VMED in this study is shown in Fig. 1. The VMED consists of a glass cover, some of the plates, wicks, and a seawater feeding unit. Each effect has a cotton-cloth wick attached to one side of the plate, which serves to spread the seawater as it flows slowly from the plate. In our previous study, a single glass cover was used, but a double glazing glass cover was used to reduce heat loss by an air gap with a relatively low conductive heat transfer coefficient as mentioned earlier. The inner glass has attached black wick, which supplies seawater to evaporation surface and at the same time serves as a collector that absorbs solar radiative energy. The solar radiation penetrates the double glazing glass cover and is absorbed by the black wick attached to the inner glass. The thermal energy absorbed by the black wick increases the temperature of the seawater flowing through the wick, thus the wick's seawater is evaporated. The vapor generated at this time diffuses to the next plate 5 mm apart, which is optimum value from the previous study [14], and then is condensed on the surface of the next plate because of its relatively low temperature. The condensate flows down the plate by gravity and is collected from the bottom. On the other hand, when the vapor condenses on the plate, the condensation latent heat is transferred to the plate, so that the temperature of the plate increases, and this thermal energy is transferred to the wick attached on the plate, and seawater in the wick evaporates. In this way, the fresh water is obtained by repeated evaporation, diffusion, and condensation processes from the first to the last effect. As the concentration of seawater flowing down along the wick gradually increases due to evaporation, concentrated seawater is discharged at the bottom of the wick. The last effect plate of the VMED has no wick attached and thermal energy of the last plate is released to the atmosphere by convection and radiation. The seawater supply unit is located at the upper part of the VMED and serves to supply a specified amount of seawater to the wick.

In summer solstice, the temperature of the black wick of the VMED increases over 75 °C with feed water of 25 °C [30]. The temperature of effect plates gradually decreases as going through last plate and the temperature difference between plates is within 3 °C [35].

## 3. Numerical model

### 3.1. Heat and mass transfer model

Heat and mass transfer equations of wicks and plates from black wick to the last plate in the still were described in our previous paper in detail [35]. Therefore, we only presented modified or newly added equations. Though the energy equations on plates and wicks are identical with those of the previous study, equations of the glass cover were modified due to the usage of double glass. Fig. 2 shows the flow of thermal energy in outer glass and inner glass. The energy equations for those are shown in Eqs. (1)–(2).

Eq. (3) uses to calculate the total solar irradiance reaching the outer glass of inclined VMED [36]. The solar radiant energies absorbed in the outer glass ( $\dot{Q}_{go,slr}$ ), inner glass ( $\dot{Q}_{gi,slr}$ ), and black wick ( $\dot{Q}_{w,slr}$ ) are derived from Eqs. (4)–(6) respectively as considering radiation transmittance and absorptivity of the glass cover.

$$\dot{Q}_{in,slr} = \left[ G_{dr,n} \left( \cos \beta + \sin \beta \frac{\cos \xi}{\tan \alpha} \right) + G_{df,n} \left( \frac{1 + \cos \beta}{2} \right) \right] \times A_g \quad (3)$$

$$\dot{Q}_{go,slr} = \left[ G_{dr,n} \left( \cos \beta + \sin \beta \frac{\cos \xi}{\tan \alpha} \right) + \tau_{go,df} G_{df,n} \left( \frac{1 + \cos \beta}{2} \right) \right] \times A_g \eta_g \quad (4)$$

$$\dot{Q}_{gi,slr} = \left[ \tau_{g,dr} G_{dr,n} \left( \cos \beta + \sin \beta \frac{\cos \xi}{\tan \alpha} \right) + \tau_{gi,df} G_{df,n} \left( \frac{1 + \cos \beta}{2} \right) \right] \times A_g \eta_g \quad (5)$$

$$\dot{Q}_{w,slr} = \left[ (\tau_{g,dr})^2 G_{dr,n} \left( \cos \beta + \sin \beta \frac{\cos \xi}{\tan \alpha} \right) + \tau_{w,df} G_{df,n} \left( \frac{1 + \cos \beta}{2} \right) \right] \times A_w \eta_w \quad (6)$$

In Eq. (7), the heat transfer in the gap of glass cover was presented. Heat transfer between the inner glass and outer glass is similar to that between inclined parallel plates. Therefore, the Nusselt number ( $Nu$ ) of this equation was calculated from Eq. (8) developed by Hollands et al. [37]. The  $[X]^*$  means in Eq. (8)  $(|X| + X)/2$ .

$$\dot{Q}_{c,go} = h_{a,gi-go} (T_{gi} - T_{go}), \quad h_{a,gi-go} = \frac{Nu k_a}{d} \quad (7)$$

$$Nu = 1 + 1.44 \left[ 1 - \frac{1708}{Ra \cos \beta} \right]^* \left( 1 - \frac{(\sin \beta)^{1.6} 1708}{Ra \cos \beta} \right) + \left[ \left( \frac{Ra \cos \beta}{5830} \right)^{1/3} - 1 \right]^* \quad (8)$$

(at  $\beta \leq 60^\circ$  and  $0 < Ra \leq 10^5$ )

After evaporation of seawater in the wick, the evaporated steam was diffused through the air gap to the next plate surface. A mass flow rate of the steam was calculated by Stefan's law as presented in Eqs. (9)–(10) [38]. This mass flow rate is the same as that of condensed water on next plate. The saturated water vapor pressure in Eq. (9) uses Fernandez and Chargoy's formula [39] of Eq. (11). Daily total production of VMED is calculated from Eq. (12). Table 1 shows the thermal and radiation properties used in this numerical analysis.

$$\dot{m}_e = \frac{DP_{atm}}{R_v T_m d} \times \ln \left( \frac{P_{atm} - P_{cd}}{P_{atm} - P_{ht}} \right) \quad (9)$$

$$D = 0.187 \times 10^{-9} T_m^{2.072} \quad (10)$$

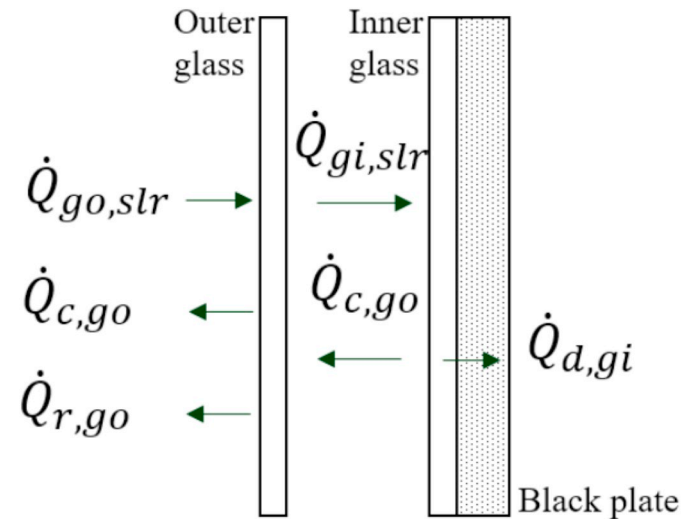


Fig. 2. Flow schematics of thermal energy in glass cover.

$$\dot{Q}_{go,slr} + \dot{Q}_{d,go} = \rho_{go} V_{go} c_{go} \frac{dT_{go}}{dt} + \dot{Q}_{c,go} + \dot{Q}_{r,go} \quad (1)$$

$$\dot{Q}_{gi,slr} + \dot{Q}_{d,gi} = \rho_{gi} V_{gi} c_{gi} \frac{dT_{gi}}{dt} + \dot{Q}_{d,go} \quad (2)$$

**Table 1**  
Radiation properties of glass and wick in VMED.

Radiation properties
·Absorptance and emittance of glass and wick $\eta_w = 0.9, \eta_g = 0.05, \varepsilon_g = \varepsilon_w = 0.9$
·Transmittance of glass $\tau_{g, dr} = 0.697 \cos^3\theta - 0.31 \cos^2\theta - 2.096 \cos\theta + 2.56 \cos\theta$ [30] ( $\cos\theta = \sin\alpha \cos\beta + \cos\alpha \sin\beta \cos\xi$ )
$\tau_{gi, df} = \tau_{w, df} = -3.395 \times 10^{-5} \times \beta^2 + 3.005 \times 10^{-3} \times \beta + 0.3275$ [11]
$\tau_{go, df} = 0.5$

$$p_v = \exp\left(25.317 - \frac{5144}{T_v}\right) \quad (11)$$

$$m_i = \sum (\dot{m}_e \times \Delta t) \quad (12)$$

### 3.2. Model verification

To verify the numerical model, we experimented on for ten-effect VMED as shown in Fig. 3. The collecting area is 0.44 m<sup>2</sup> (0.54 m × 0.82 m). The gap distance of the double glass cover is 20 mm and those have 3 mm thickness. The first wick is colored by black. Thicknesses of all cotton fabric wicks and STS 316 L plates are 0.1 and 0.5 mm, respectively. The gap distance between the effects is 5 mm. In the saline water feed unit positioned on top of the VMED, the float valve is installed to maintain constant water level. The wick submerged in the tank sucks up the saline water by capillary force and then flows down naturally by gravity to supply saline water to the VMED. At this time, since the level of the water tank is constant, the feed flow rate to VMED can be also continuous at 12 g/min as a target flow rate. The schematics of the test equipment of the VMED is presented in Fig. 4. The pyranometer, anemoscope, and anemometer were installed to measure environmental conditions such as solar insolation, wind direction, and wind speed. K-type thermocouples were installed to measure the temperatures of wicks, plates, and ambient. Table 2 shows the list of all measuring instruments used in this study. Measurement uncertainty of instruments is evaluated by B-type standard uncertainty.

The performance test was conducted six times during November 6–13, 2017. The VMED test equipment was installed in South Korea (N35.27°, E128.77°). Table 3 shows the environmental conditions in the experiment. In addition, the productivities calculated from the numerical analysis were compared. In Fig. 5, the productivities obtained from experiments and numerical analysis were compared according to test dates. The root mean square error (RMS error) from two result data was found to be 0.39 kg/(m<sup>2</sup>·d). In Fig. 6, as a result of comparing the slope of the linear fitting lines from the graph with production vs. total solar radiation, the difference between the two slopes was only 0.5%. Therefore, it was confirmed that the numerical results for the VMED were in good agreement with the experimental results.

## 4. Results and discussion

### 4.1. Analysis conditions

Considering on the four seasons of South Korea, the spring equinox, summer solstice, autumn equinox, and winter solstice representing the environmental conditions of each season were selected as the reference dates. Table 4 presents the environmental conditions such as seasonal air temperature, sunrise/sunset time and global insolation. The size of the VMED components is shown in Table 5. The effective area of the VMED is 1 m<sup>2</sup> based on the collecting area for solar radiation. The thicknesses of each glass, plate and wick are 5, 0.5, and 0.1 mm, respectively, and the spacing between effects is 5 mm. Table 6 presents the variables to be considered in the numerical analysis and the range

of values of those. When analyzing the performance characteristics according to the target variables, other variables used default values in parentheses as presented in Table 6. The default values applied to numerical analysis were indicated at the top side in the result graphs.

### 4.2. Gap distance of double glass cover

The heat transfer rate in the gap of the double glass is changed according to the gap distance and the slope of the glass as presented in the Eqs. (7) to (8). Therefore, it is necessary to optimize the gap distance of double glass cover to increase the production efficiency of the VMED. The analysis results for deriving the optimum spacing of double glass are shown in Fig. 7. The results showed that as the gap distance increased from 2 to 35 mm, the production increased by 4.0, 9.0, 4.5 and 0.6 kg/(m<sup>2</sup>·d) in spring, summer, autumn and winter, respectively. But the average output scarcely increased after the gap distance of 30 mm. If the distance between the double glass increases 25 to 30 mm, the average production increases only by 1.6%. As the gap distance increases, the sealing thickness of glass sides increases, so that the shadow interference to the thermal collecting surface increases further. It is recommended to keep it at 25–30 mm for gap distance of double glass cover.

### 4.3. Number of effects

The numerical analysis results according to the number of effects ( $N_t$ ) were presented in Fig. 8. As the  $N_t$  increased, freshwater production also increased and then appeared to be constant. The results showed that the minimum numbers of effects for the maximum production ( $N_{t,min}$ ) were 20, 30, 20, and 10 in the spring, summer, autumn, and winter, respectively. The productivity at the  $N_{t,min}$  increased by 2.88, 4.45, 3.23 and 1.96 times, respectively of that at  $N_t = 2$ . From this result, it can be seen that the higher the amount of insolation is, the higher the production increases according to  $N_t$ , and more  $N_t$  is required to obtain the maximum production. Increasing  $N_t$  yields more output, but increases the cost of manufacturing, maintaining, and repairing the utility. Therefore, it is necessary to determine the optimal  $N_t$  through economic analysis considering all these points. To determine the optimal  $N_t$ , the payback period and yearly net profit were analyzed. Table 7 shows the values to calculate production cost, maintenance cost, and yearly net profit. After all, the payback period can be derived



Fig. 3. Ten-effect VMED for performance test.

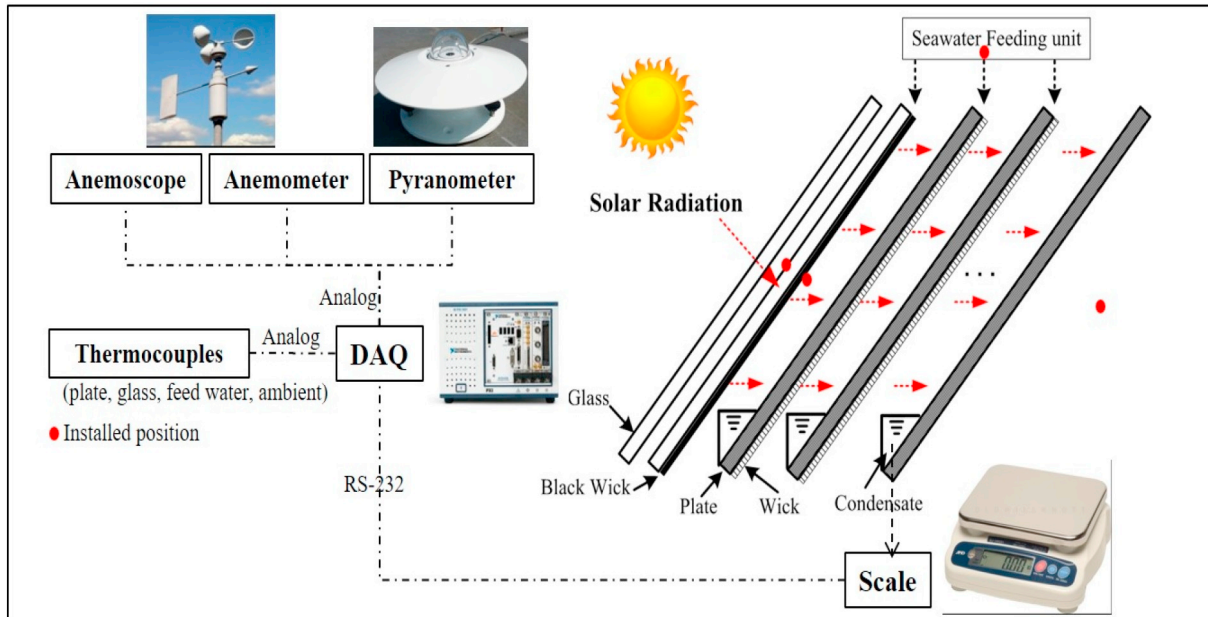


Fig. 4. Schematics of performance test equipment.

**Table 2**  
Specifications of measuring instruments for performance test.

Instrument	Measuring range	Accuracy	Standard uncertainty
Pyranometer	0–2800 W/m <sup>2</sup>	1 W/m <sup>2</sup>	0.58 W/m <sup>2</sup>
Anemoscope	0–50 m/s	0.1 m/s	0.06 m/s
Anemometer	0–360°	2°	0.2°
T-type Thermocouple	–270–370 °C	0.1 °C	0.06 °C
Scale	0–3.0 kg	0.1 g	0.06 g

**Table 3**  
Climate conditions in performance test.

Date for experiments (dd-mm-yy)	$Q_{gb}$ , MJ/m <sup>2</sup>	$T_{amb}$ , °C	Wind speed, m/s
06-11-17	12.53	13.1	1.0
07-11-17	8.53	13.1	0.8
08-11-17	11.6	20.6	1.7
09-11-17	11.59	16.0	0.98
10-11-17	9.79	18.0	1.75
13-11-17	10.22	12.64	1.23

by substituting  $N_b$ , maintenance cost, yearly net profit, and annual average output into the formula shown in Table 7. Bottled water cost is considered 0.3–0.6 \$/kg considering on various nations [40–43]. Fig. 9 shows the analysis results on the payback period and yearly net profit which were based on the average production of four seasons with  $N_t$  as shown in Fig. 8. Yearly net profit was calculated by subtracting production and maintenance costs from total sales profit of water presented in Table 7. Regardless of the water cost, the payback period is the minimum when the  $N_t$  is 6–8, and the maximum yearly net profit is when the  $N_t$  is 20. In Fig. 9, however, the payback period in the range of  $N_t = 6$ –10 or yearly net profit of more than  $N_t = 15$  is similar. From these results, the optimal  $N_t$  of 10–15 considering both the payback period and the yearly net profit is appropriate.

On the other hand, as shown in Fig. 9, when the water cost is 0.3 \$/kg, the payback time is about 1 year in the optimal  $N_t$ . In the Middle East, the payback time will be reduced to within 8 months because the operating days are over 300 days/yr (1.5 times longer than in Korea) and solar irradiance is higher than other countries.

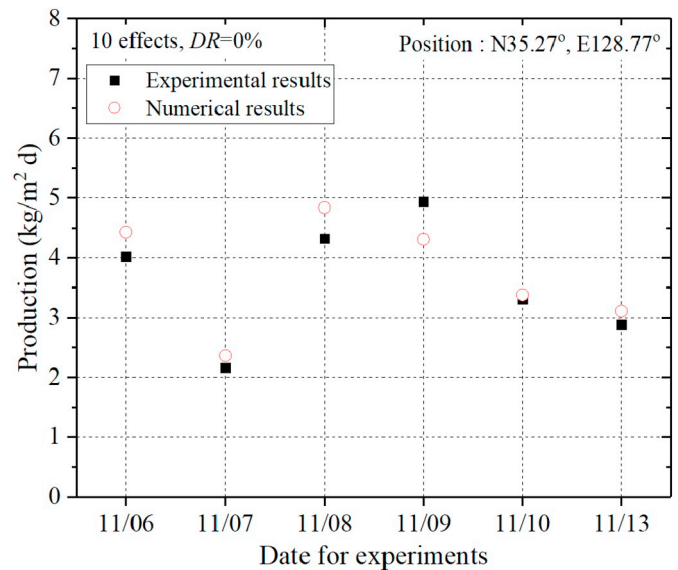


Fig. 5. Comparison with experimental and numerical results (production vs. date for experiments).

#### 4.4. Effect plate materials

The plate of the VMED functions as a condensation surface for condensing the humid vapor, and also serves to transfer the latent heat of the condensates to the wick attached to the opposite side. The amount of condensation increases as the temperature difference increases and the temperature is higher as shown in Eqs. (9)–(11). Moreover, the higher the heat transfer rate of the plate is, the higher the efficiency of the VMED is. Therefore, the thermal conductivity of the plate material affects the performance of the VMED. In this study, the basic material of the plate was considered as STS 316 L, but various metal and non-metallic materials such as Aluminum, Nickel, Carbon steel, thermally conductive plastic and PET (Poly-Ethylene Terephthalate) can also be applied to the plate of the VMED. Fig. 10 shows the numerical results of production for various materials of the plate. In this analysis, the all the plates kept the same thicknesses at 0.5 mm.

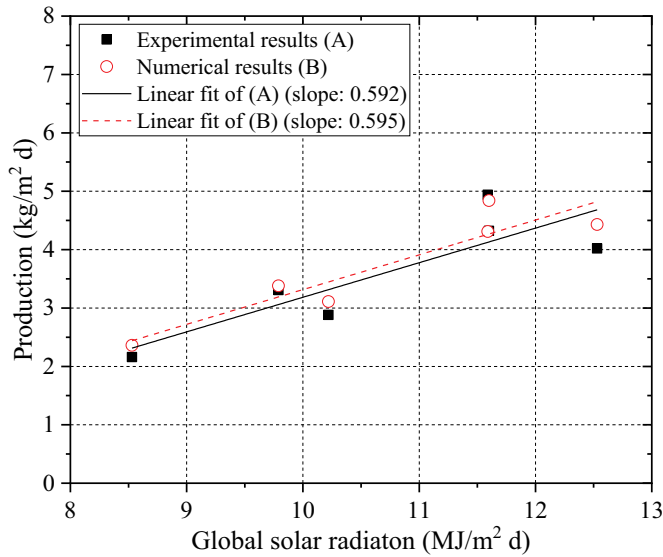


Fig. 6. Comparison with linear fitting slopes of experimental and numerical results (production vs. global solar radiation).

Table 4  
Numerical conditions for four seasons.

Seasons	Conditions				
	Representative Date [mm/dd]	$T_{atm}$ , °C	Sunrise	Sunset	Global insolation, MJ/m <sup>2</sup> d
Spring	3/20	15	AM 6:42	PM 18:38	16.1
Summer	6/21	30	AM 5:18	PM 19:49	25.1
Fall	9/23	22	AM 6:25	PM 18:22	15.8
Winter	12/22	10	AM 7:45	PM 17:17	6.0

Table 5  
Size of the VMED components.

Component list	Size
Glass and plate size	1 m(W) × 1 m(H) = 1 m <sup>2</sup>
Glass thickness	5 mm
Plate thickness	0.5 mm
Wick thickness	0.1 mm
Gap distance between effects	5 mm

Table 6  
Numerical parameters and the default value of fixed variables.

Parameters	Values of variable (default value)
Gap distance of double glass cover	2–30 mm (20)
The number of effects	2–30 (10)
Materials of plate	STS 316 L, Al, Carbon steel, Ni, Thermally conductive plastic, PET (STS 316L)
Feed flow rate	6–25 g/min (25)
Decreasing rate	0%, 2%, 4% (0)

Among the plate materials, the highest production was obtained at the aluminum plate in which the thermal conductivity is 16.9 times than STS 316L, but the difference in the production compared to when using STS 316L was as small as 0.05%. The production decreased by up to 4.8% and 7.7%, respectively, when using thermally conductive plastic and PET, which have much lower thermal conductivity than STS 316L. If changing the thickness of the plate, it is necessary to analyze from viewpoint of the conductive thermal resistance. Conductive thermal resistance of materials is proportional to thickness and inversely

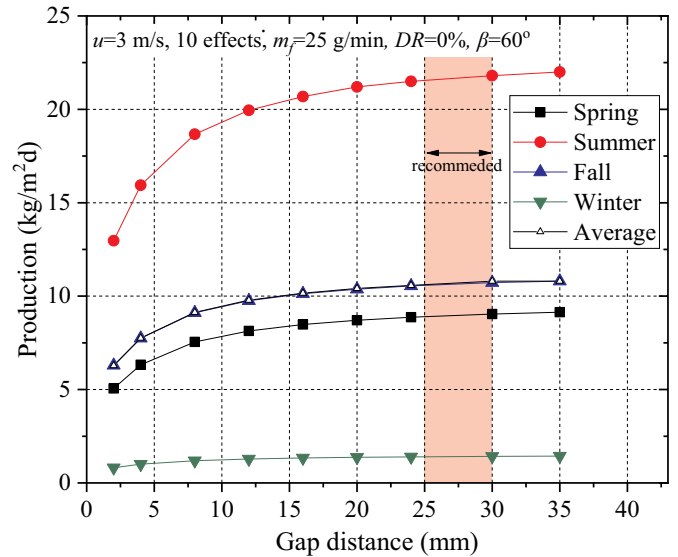


Fig. 7. Numerical results for production with gap distance of double cover glass.

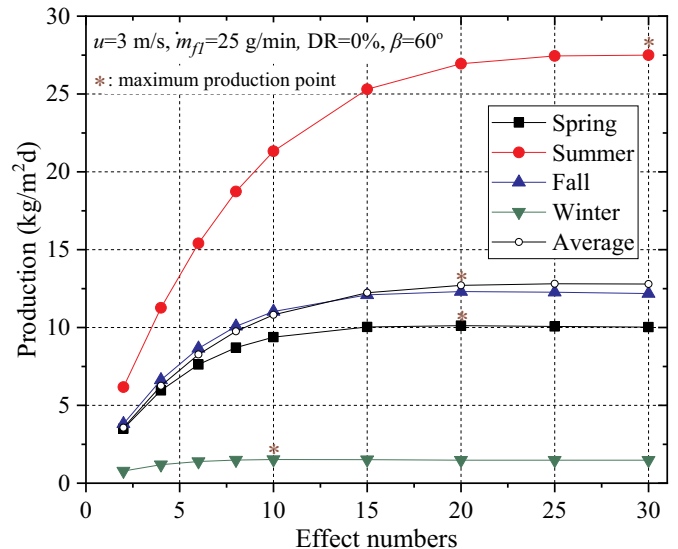


Fig. 8. Numerical result for production with effect number of the MED.

proportional to thermal conductivity and area. The conductive thermal resistance of STS 316L plate with a thickness of the 0.5 mm is  $3.57 \times 10^{-5}$  K/W as presented in Eq. (13) [38].

$$R = \frac{d}{k \times A} = \frac{0.0005 \text{ m}}{14 \text{ W/(m K)} \times 1\text{m}^2} = 3.57 \times 10^{-5} \text{ K/W} \quad (13)$$

In the same way, the thermal resistances of a thermally conductive plastic and PET are 0.0001 and 0.005 K/W, respectively, which is about 28–140 times higher than that of STS 316L. As shown in the previous results, this material reduces production by 4.8–7.7% compared to STS 316L. Therefore, to achieve the same output, it should be designed to be lower than  $3.57 \times 10^{-5}$  K/W, the thermal resistance of STS 316L. If the thickness of the thermally conductive plastic is reduced to 0.1 mm, the conductive thermal resistance is  $2.0 \times 10^{-5}$  K/W, which is lower than the value of STS 316L, so that a similar product can be obtained like as STS 316L. Since PET has a thermal conductivity of 0.1 W/(m·K), a PET film of  $3.57 \times 10^{-3}$  mm should be used to achieve the same thermal resistance as STS 316 L with 0.5 mm thickness.

In order to analyze the reason why the change in production was

**Table 7**  
Production and maintenance cost for the VMED.

Production cost (A)			
Components	Unit price, \$	Number	Cost, \$
Double glass (low iron)	50	1	50
STS 316 L plate	30	$N_t$	$30 \times N_t$
Fabric wick	1	$N_t$	$1 \times N_t$
Hot melt adhesive film	1	$N_t$	$1 \times N_t$
Seawater feed unit	30	1	30
Case	30	1	30
Leak proof silicone	1.96	$N_t$	$1.96 \times N_t$
Filter system	50	1	50
Accessories	5	1	5
Production cost, \$			$33.96 \times N_t + 165$
Maintenance cost (B)			$A \times 0.15$
Daily average production		$C$	kg/d
Operation days in year		200	days/yr
Yearly total production (D)		$200 \times C$	kg/yr
Water cost (E)		0.3, 0.45, 0.6	\$/kg
Yearly sales profit of water (F)		$D \times E$	\$/yr
Yearly net profit		$F - B$	\$/yr
Payback period		$A / (F - B)$	yr

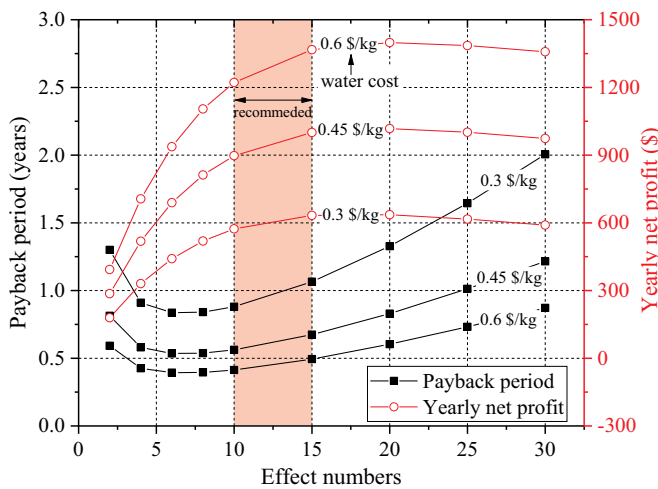


Fig. 9. Payback period and yearly net profit with effect numbers.

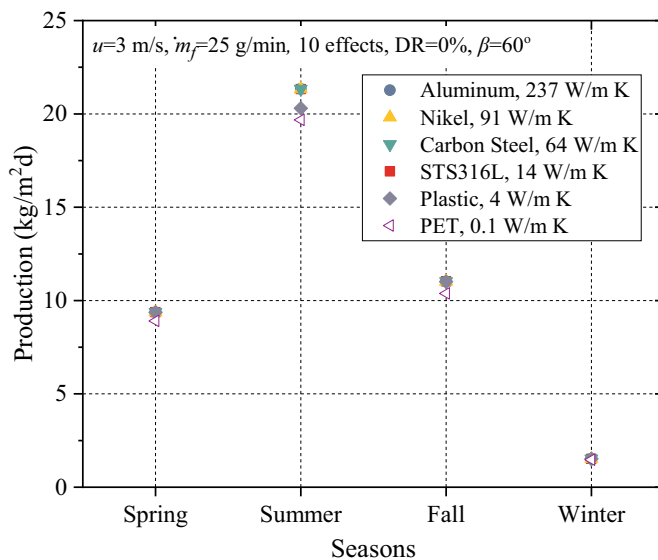


Fig. 10. Seasonal production with materials of the MED plate.

insignificant despite the increase in the thermal conductivity of the plate material, temperature difference inside the plate was analyzed at the maximum input heat flux condition. The input heat flux was the maximum value of  $375 \text{ W/m}^2$  in summer. The temperature difference of the 0.5 mm STS 316 L plate was  $0.013 \text{ }^\circ\text{C}$  as shown in Eq. (14) [38].

$$\Delta T = \frac{d}{k \times A} \times \dot{Q} = \frac{0.0005 \text{ m}}{14 \text{ W/m} \times 1\text{m}^2} \times 375 \text{ W/m}^2 = 0.013^\circ\text{C} \quad (14)$$

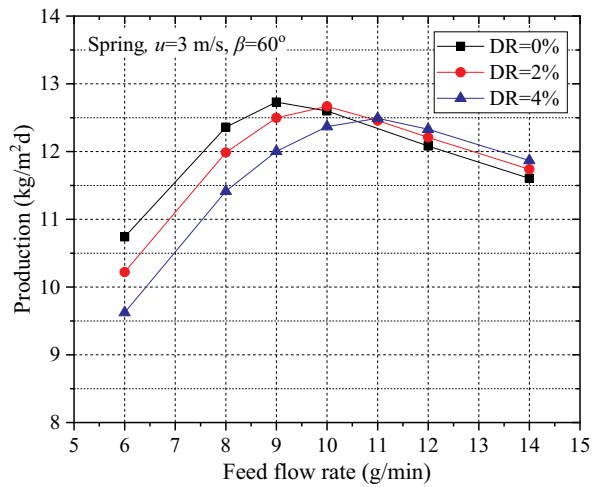
In the same manner, the temperature differences of the plates with aluminum, thermally conductive plastics and PET were  $7.9 \times 10^{-4} \text{ }^\circ\text{C}$ ,  $0.047 \text{ }^\circ\text{C}$  and  $1.88 \text{ }^\circ\text{C}$ , respectively in summer. In the case of spring, autumn, and winter, whose heat flux is lower than the summer, the temperature difference of plates according to each material is further reduced and the variation of the production by plate materials was reduced as shown in Fig. 10. After all, considering the temperature difference according to the heat flux supplied to the plate, even though the thermal resistance is lower than the STS 316L, the increase in production is insignificant.

In summary, even if the plate's thermal resistance is lower than that of 0.5 mm thick STS 316L, that is  $3.57 \times 10^{-5} \text{ K/W}$ , the increase in production is negligible. If the PET flat plate is used in the VMED, the average annual output will be reduced by 6.49% compared to the STS 316L plate, but the manufacturing cost will be reduced. Therefore, economic analysis will be needed for the application of the plates with nonmetallic materials in the VMED, which is described in subsequent section.

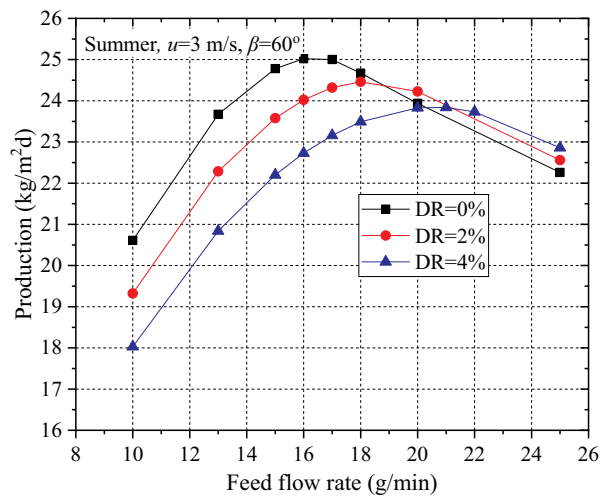
#### 4.5. Feed flow rate

Fig. 11 shows the numerical result for production with the feed flow rate ( $m_f$ ) and decreasing rate (DR) to find optimum flow condition to the VMED. The DR means the ratio of decrease of the feed flow rate supplied to each effect to the next effect. At the feed flow rate of  $\text{DR} = 0\%$  (which means feeding at the same flow rate to all the effects), the productivities were 10.7–12.7, 20.6–25.0, 11.4–14.5, and 1.6–2.3  $\text{kg}/(\text{m}^2\text{-d})$ , respectively at spring, summer, autumn, and winter. As shown in Fig. 11, there was an optimum  $m_f$  to obtain the maximum production in each season. At  $\text{DR} = 0\%$ , the optimum values were 9, 16, 10, and 3  $\text{g}/\text{min}$  in spring, summer, autumn, and winter, respectively, and increased with solar radiation. The reasons for low production when the feed flow rate is not optimal are as follows. If the  $m_f$  exceeds over optimum value, relatively cold feed water will lower the seawater temperature flowing the wick further, and evaporation rate will decrease. On the contrary, if the  $m_f$  is less than optimum value, the evaporation rate from wick exceeds the feed rate of seawater, and dry-out of the wick may occur locally. In this case, as the evaporation area of the wick decreases, not only the productivity will decrease, but also the salt will be precipitated at wick surface, which may cause adverse effects such as aging, desorption, and corrosion. Considering the reduction slope when  $m_f$  is out of optimal values, it is advantageous to supply a little more than optimum  $m_f$  for stable operation.

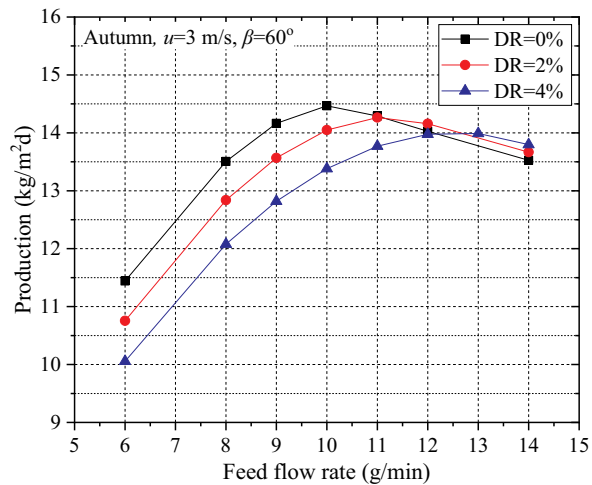
As the DR increased, the optimum  $m_f$  increased but the maximum production decreased except for winter. As shown in Fig. 11(b), the optimum value was 16  $\text{g}/\text{min}$  when  $\text{DR} = 0\%$ , but increased to 18 and 21  $\text{g}/\text{min}$ , respectively, when  $\text{DR} = 2\%$  and  $4\%$ . The maximum production decreased gradually from 25.0 to 24.5 and 23.8  $\text{kg}/(\text{m}^2\text{-d})$  with the increase of the DR. This result, which the VMED got the maximum output at  $\text{DR} = 0\%$ , is not match with the findings of Tanaka et al. [44]. The previous study has suggested that to increase the efficiency of the VMED, and it is better to gradually reduce the seawater supply ( $\text{DR} > 0\%$ ) from the first to the last effect. In order to elucidate the reasons for these conflicting results, we analyzed production with DR (0–12%) as shown in Fig. 12. The results showed that the production profiles with the DR varied with  $m_f$ . The production continued to decrease as DR increased at  $m_f = 16$  and 18  $\text{g}/\text{min}$ , which were close to optimum  $m_f$  (16.0  $\text{g}/\text{min}$ ). However, at  $m_f = 25$  and 30  $\text{g}/\text{min}$  above



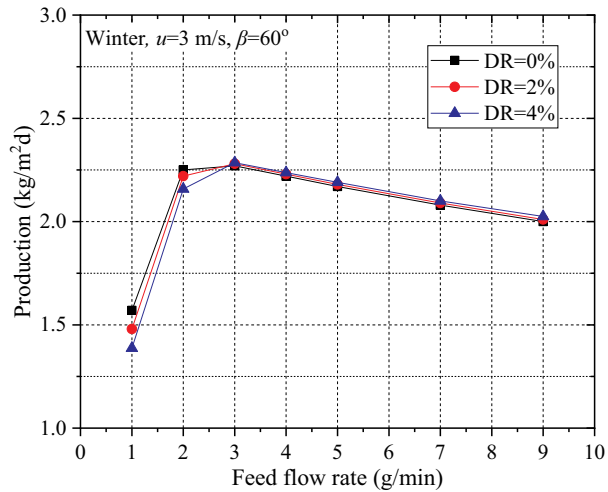
(a) Spring



(b) Summer



(c) Autumn



(d) Winter

Fig. 11. Production with a feed flow rate in each season.

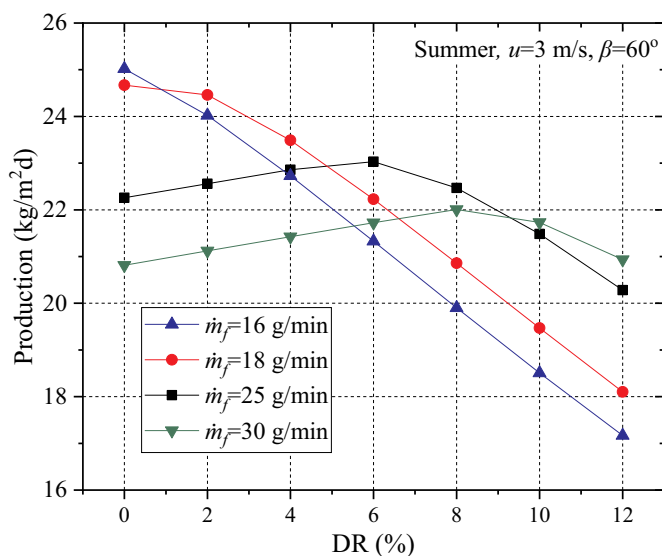


Fig. 12. Production with DR at a specified feed flow rate.

the optimum  $\dot{m}_f$  of DR = 0%, the DR for maximum output was 6% for  $\dot{m}_f = 25$  g/min and 8% for  $\dot{m}_f = 30$  g/min. It means that the DR to get the maximum production may exceed 0% in overfull  $\dot{m}_f$ . When the  $\dot{m}_f$  is 1.6 times more than the optimum feed flow rate (16.0 g/min) of DR = 0%, it follows the trend suggested by the previous study [44], but when the  $\dot{m}_f$  is close to the optimum flow rate, it is better to flow the same feed rate to each effect, that is DR = 0%. These results are valuable because it ensures operational convenience and the design simplicity of the seawater supply unit.

Depending on the operating conditions of the VMED, it may be necessary to keep a constant feed flow rate regardless of the season. In consideration of these conditions, the daily average product in a year was analyzed according to the feed flow rate. As shown in Fig. 13, the optimum  $\dot{m}_f$  is 14 g/min at  $\beta = 60^\circ$  and 8 g/min at  $\beta = 90^\circ$ , where each production is 12.8 and 6.7 kg/(m<sup>2</sup>·d). The decrease in production at the  $\dot{m}_f$  outside the optimum value was more gentle at  $\beta = 60^\circ$  than  $\beta = 90^\circ$ . It can be seen that the higher solar irradiation to the VMED is, the less the variation of the production with  $\dot{m}_f$  is. Production change for the flow rate of 11 to 17 g/min at  $\beta = 60^\circ$  is within 1.8% of the maximum production. This range includes the optimum flow rate ( $\dot{m}_f = 16$  g/min) to obtain the maximum production in summer as presented in Fig. 11. Therefore, in operating conditions that supply the

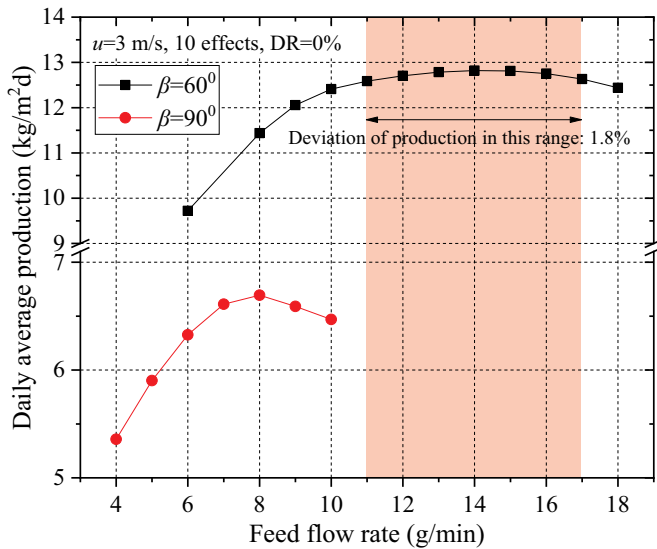


Fig. 13. Daily average production with a feed flow rate in a year.

same feed flow rate throughout the year, it is preferable to provide the value of the optimum  $m_f$  at the maximum solar irradiation condition.

### 5. Optimum conditions and maximum production

Table 8 summarizes the optimal values of the design and operation parameter of the VMED from previous analysis results. In the previous study [35], the optimum inclination in the ground of the VMED was presented as 40–50°. In this numerical analysis for the maximum production, the applied values for gap distance of glass cover, the number of effects, and inclination are 25 mm, 15, and 40°, respectively. Numerical results with these optimum conditions show that productivities in spring, summer, autumn, and winter are 16.6, 36.0, 19.0 and 2.5 kg/(m²·d), respectively. The average annual production is 18.5 kg/(m²·d) and increased 1.1–1.4 times higher than the average of seasonal maximum productions presented in Fig. 10. Moreover, the maximum production is higher 2.1 times than that in our previous study [35]. The performance ratio (PR) is a term that indicates how effectively the supplied solar energy is used by the solar still for producing distilled water [45]. Cooper [7] theoretically found that the maximum PR of the CSS was below 0.6. The PR of the VMED of this study was the highest as 3.58 in summer, and was 2.03, 2.35, and 0.69 in spring, autumn, and winter, respectively. Under optimum conditions, the recovery rate of the VMED was 30.0–35.8%.

### 6. Economic analysis

Economic analysis was performed to compare the competitiveness of this VMED with other solar stills. The water cost was necessary to derive for the economic analysis of the solar still and was calculated using the following Eqs. (15)–(20) [46,47].

$$SFF = \frac{i}{[(1 + i)^n - 1]} \tag{15}$$

$$CRF = SFF \times (1 + i)^n \tag{16}$$

$$FAC = (PC) \times (CRF) \tag{17}$$

$$ASV = (SFF) \times SV, SV = 0.2 \times (PC) \tag{18}$$

$$AC = FAC + AMC - ASV, AMC = 0.15 \times FAC \tag{19}$$

$$CPT = AC/M \times 1000 \tag{20}$$

where SFF is the sinking fund factor, CRF is the capital recovery factor,

FAC is fixed annual cost, PC is present capital cost, ASV is the annual salvage value, SV is salvage value, AC is the annual cost, AMC is the annual maintenance operational cost, and M is annual production, CPT is the cost of distilled water per ton. The M is calculated by multiplying the average annually production by solar irradiance 200 days in a year considering the climate conditions of South Korea. For comparison with other solar stills, the same values were used for interest rates  $i$  of 12% and  $n$  of 10 years. Table 9 shows the economic analysis results of our VMED and the other solar stills [48]. The CPT for the our optimized VMED in Section 5 was 35.0 \$/m³.

Considering that the CPT range of other solar stills was 9.9–64.6 \$/m³, the CPT of our VMED was near to an average value. It was necessary to lower the manufacturing cost of \$674.4 to reduce the CPT of this VMED. This was because it was 3.1 times higher than the average manufacturing cost of \$217.5 for other solar stills. As shown in Table 7, the most expensive part of our VMED was the plates with STS 316L. Therefore, changing the plate material can be considered as a way to lower manufacturing costs. In Section 4.4, we presented that the production of VMEDs was almost similar when the conductive thermal resistance of the VMED plates was lower than that of 0.5 mm thick STS 316L. Therefore, even though the material of the plate is replaced with cheaper thermally conductive plastic or PET with a thickness of < 0.5 mm, the output of VMED will be almost not changed. The annual average productivities of the VMEDs with the thermally conductive plastic and PET plate of 0.1 mm thickness were 18.5 and 18.4 kg/(m²·d), respectively, by resulting from the numerical analysis under optimum conditions presented in Table 9. The unit costs for thermally conductive plastics and PET plate with 1 m² area and 0.1 mm thickness are 10 \$/piece and 6 \$/piece, respectively, and considering these, the production costs of the VMED are \$374.4 and \$314.4, respectively. The CPT of this VMED with nonmetallic plates will be 16.4–19.4 \$/m³, saving about 53.4% from the existing CPT (35.0 \$/m³).

However, it is necessary to compare CPT of the VMED with those of other types of solar desalination systems such as RO, MD, MED, and etc. to be competitive in the market. In particular, it is necessary to analyze the CPT considering on the decrease in CPT with production capacity. Fig. 14 shows the CPT with the capacity of various solar desalination systems presented in the previous study [3]. The CPTs of solar still presented in Table 9 were included in this graph and the capacity of those was assumed to 0.1 m³/d. Moreover, based on the data of Fig. 14, the average CPT within a specific capacity range was presented for a clear comparison in Fig. 15. The Roman alphabet (I–III) in Figs. 14 and 15 represent for VMEDs considering on various conditions to lower the CPT. The Roman alphabet ‘I’ means the VMED with STS 316L plate as a reference model. In the previous economic analysis, we applied interest rates of 12% and lifetimes of 10 years to compare with other solar stills, but these might not be realistic values. In South Korea, the interesting rate for project financing is about 6.5–10% depending on credit rating, and the recommended lifetime of solar stills should be normally about 20 years [49]. By considering these, the CPT of the VMED is reduced to 10.0–13.3 \$/m³ (II). Moreover, if the VMED is installed in the Middle East such as Kuwait or Saudi Arabia, the solar irradiance days in a year will increase by 330 days (from climate data of www.meteoblue.com).

Table 8 Optimum conditions for design and operation parameter of VMED.

Parameters		Optimum conditions	
Design parameters	Gap distance of glass cover, mm	25–30	
	The number of effects, #	10–15	
Operation parameters	Inclination in the ground, °	40–50 [35]	
	Seasonal feed flow rate, g/min	In spring	9
		In summer	16
		In fall	10
		In winter	3
Decreasing rate of feed flow rate	0%		

**Table 9**  
Cost analysis of this study compared with other types of solar desalination systems [48].

Type of solar still	PC, \$	FAC, \$	SV, \$	ASV, \$	AMC, \$	AC, \$	M, kg/yr	CPT, \$/m <sup>3</sup>	
This study	STS 316L plate	674.4	119.4	134.9	7.69	17.9	129.58	3700	35.0
	Thermally conductive plastic plate	374.4	66.26	74.9	4.27	9.94	71.94	3700	19.4
	PET plate	314.4	55.64	62.88	3.58	8.35	60.41	3680	16.4
VMED with collector	1077	190.6	215.4	12.3	28.6	206.9	5330	38.8	
Double effect CSS	164	29.03	32.8	1.87	4.35	31.51	775	40.7	
Double effect double slope CSS	160.6	28.42	32.12	1.83	4.26	30.86	1235	25.0	
Double effect CSS with heat exchanger	319	56.46	63.8	3.64	8.47	16.29	1152	53.2	
Double effect CSS with vacuum tubes	194.7	34.46	38.94	2.22	5.17	37.41	1056	35.4	
Triple effect CSS	170	30.09	34	1.94	4.51	32.66	3285	9.9	
Triple-effect tubular still	299	52.92	59.8	3.41	7.94	57.45	1592	36.1	
Single effect still with wick	150	26.55	30	1.71	3.98	28.82	1058	27.2	
Single effect still with fin	165	29.2	33	1.88	4.38	31.7	731	43.4	
Fin-type still	160	28.32	32	1.82	4.25	30.74	720	42.7	
Stepped still with collector	469	83	93.8	5.35	12.5	90.11	1394	64.6	
Stepped still with internal reflector	136	24.07	27.2	1.55	3.61	26.13	1326	19.7	
Still with vapor adsorption basin	223	39.47	44.6	2.54	5.92	42.85	962	44.5	
Average CPT of different type of solar still								37.0	

Then, the CPT of this VMED decreases by 6.1–8.1 \$/m<sup>3</sup> (III).

As shown in Fig. 14, the water cost of solar desalination systems decreased as the water production capacity increased. The capacity where the water cost of the VMED (III) intersects with the fitting line in the graph is about 10 m<sup>3</sup>/d. Moreover, when comparing the average water cost in Fig. 15, the VMED (III) is 48.6–52.9% cheaper than others with 1–100 m<sup>3</sup>/d. In particular, it is 81.7% cheaper than others below 1 m<sup>3</sup>/d. This shows that our VMED is more competitive in the solar desalination market of the production capacity of < 100 m<sup>3</sup>/d. However, for large capacity over 10<sup>4</sup> m<sup>3</sup>/d, solar pond-MED, solar pond-MSF, or solar assisted hybrid desalination are more competitive.

**7. Conclusions**

In this study, we focused on finding the maximum productivity by optimizing VMED and lowering the water cost of that than other solar stills. This VMED had excellent productivity and was superior to other solar desalination systems in price competitiveness. Economic analysis showed that the best water price of our VMED was 6.1 \$/m<sup>3</sup> which was

more competitive in the market than other solar desalination systems with a small capacity of < 100 m<sup>3</sup>/d. Therefore, the VMED may be more useful in remote areas with low population density and abundant solar energy.

We found the optimum conditions for the gap distance of double glass cover, the number of effects, the seawater feed flow rate, and the decrease rate of feed flow rate between effects. Moreover, these optimum conditions led to the maximum production of the 15-effect VMED. The maximum production was 16.6, 36.0, 19.0, and 2.5 kg/(m<sup>2</sup>·d) in spring, summer, autumn, and winter, respectively, and the average annual production was 18.5 kg/(m<sup>2</sup>·d) in South Korea.

The optimum feed flow rates of the VMED with collecting area of 1 m<sup>2</sup> are 9, 16, 10 and 3 g/min in spring, summer, autumn and winter, respectively, but considering the stable and reliable production for long term, it is better to supply flow rate of 1–2 g/min more. When operating near the optimum feed flow rate, it is more advantageous to supply the same flow rate to all effects. The optimal numbers of effects are 10–15 units considering both the yearly net profit and payback period. For the compactness and management convenience of the VMED,

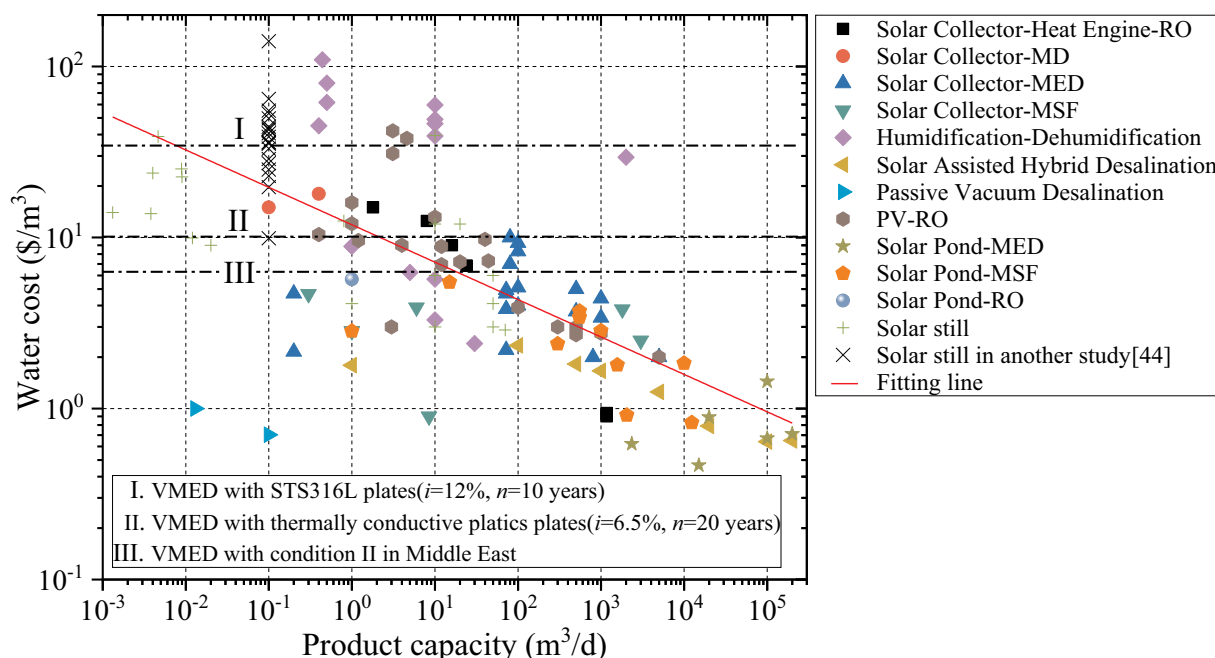


Fig. 14. Water cost with production capacity of solar desalination systems [3,48].

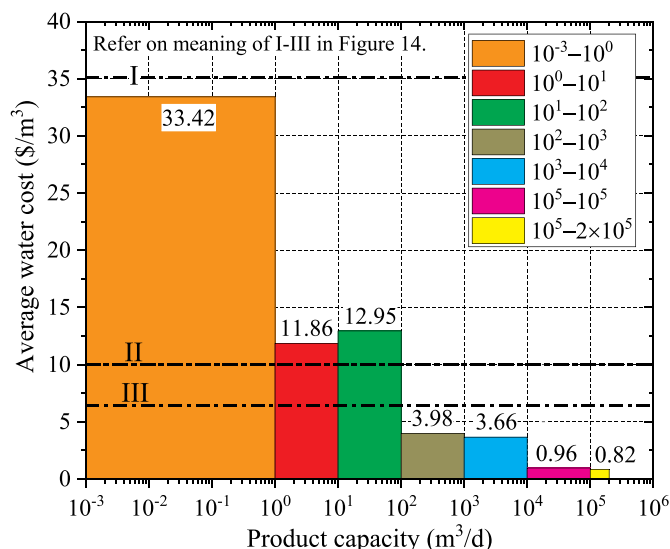


Fig. 15. Average water cost with a production capacity of solar desalination systems.

decreasing of the number of effects will be more advantageous, and 10 effects are better from a practical point of view. Optimal gap distance of double glass cover is 25–30 mm.

#### Funding sources

All funding sources for this study are listed in the “Acknowledgments” section of the manuscript.

#### CRediT authorship contribution statement

**Byung-Ju Lim:**Methodology, Data curation, Writing - original draft, Supervision, Formal analysis, Software.**Ga-Ram Lee:**Investigation, Writing - review & editing, Software, Validation.**Seok-Min Choi:**Data curation, Writing - review & editing, Formal analysis.**Kyung-Yul Chung:**Investigation, Visualization, Writing - review & editing.**Chang-Dae Park:**Methodology, Visualization, Writing - review & editing, Project administration, Validation.

#### Acknowledgements

This study was conducted with support from the Korea Institute of Energy Technology Evaluation and Planning (KETEP) and funded by the Ministry of Trade, Industry and Energy, Republic of Korea in 2017 (No. 20173030083420).

#### Declaration of Competing Interest

The authors declare that they have no known competing financial interests or personal relationships that could have appeared to influence the work reported in this paper.

#### References

- [1] A. Bajpayee, T. Luo, A. Muto, G. Chen, Very low temperature membrane-free desalination by directional solvent extraction, *Energy Environ. Sci.* 4 (2011) 1672, <https://doi.org/10.1039/c1ee01027a>.
- [2] P. Zanganeh, A.S. Goharrizi, S. Ayatollahi, M. Feilzadeh, Productivity enhancement of solar stills by nano-coating of condensing surface, *Desalination* 454 (2019) 1–9, <https://doi.org/10.1016/j.desal.2018.12.007>.
- [3] C. Li, Y. Goswami, E. Stefanakos, Solar assisted sea water desalination: a review, *Renew. Sust. Energ. Rev.* 19 (2013) 136–163, <https://doi.org/10.1016/j.rser.2012.04.059>.
- [4] R. Einav, K. Harussi, D. Perry, The footprint of the desalination processes on the environment, *Desalination* 152 (2003) 141–154, [https://doi.org/10.1016/S0011-9164\(02\)01057-3](https://doi.org/10.1016/S0011-9164(02)01057-3).
- [5] M. Feilzadeh, M.R. Karimi Estahbanati, K. Jafarpur, R. Roostaazad, M. Feilzadeh, H. Taghvaei, Year-round outdoor experiments on a multi-stage active solar still with different numbers of solar collectors, *Appl. Energy* 152 (2015) 39–46, <https://doi.org/10.1016/j.apenergy.2015.04.084>.
- [6] O. Bait, M. Si-Ameur, Tubular solar-energy collector integration: performance enhancement of classical distillation unit, *Energy* 141 (2017) 818–838, <https://doi.org/10.1016/j.energy.2017.09.110>.
- [7] P.I. Cooper, The maximum efficiency of single-effect solar stills, *Sol. Energy* 15 (1973) 205–217, [https://doi.org/10.1016/0038-092X\(73\)90085-6](https://doi.org/10.1016/0038-092X(73)90085-6).
- [8] R.A. Gupta, S.N. Rai, G.N. Tiwari, Transient analysis of double basin solar still with intermittent flow of waste hot water in night, *Energy Convers. Manag.* 28 (1988) 245–249, [https://doi.org/10.1016/0196-8904\(88\)90030-1](https://doi.org/10.1016/0196-8904(88)90030-1).
- [9] M. Kudret Selçuk, Design and performance evaluation of a multiple-effect, tilted solar distillation unit, *Sol. Energy* 8 (1964) 23–30, [https://doi.org/10.1016/0038-092X\(64\)90007-6](https://doi.org/10.1016/0038-092X(64)90007-6).
- [10] P.I. Cooper, J.A. Appleyard, The construction and performance of a three-effect, Wick-type, tilted solar still, *Sun Work* 12 (1967) 4–8.
- [11] M.M. Elsayed, K. Fathalah, J. Shams, J. Sabbagh, Performance of multiple effect diffusion stills, *Desalination* 51 (1984) 183–199, [https://doi.org/10.1016/0011-9164\(84\)85005-5](https://doi.org/10.1016/0011-9164(84)85005-5).
- [12] R. Ouahes, C. Ouahes, P. Le Goff, J. Le Goff, A hardy, high-yield solar distiller of brackish water, *Desalination* 67 (1987) 43–52, [https://doi.org/10.1016/0011-9164\(87\)90230-X](https://doi.org/10.1016/0011-9164(87)90230-X).
- [13] K. Ohshiro, T. Nosoko, T. Nagata, A compact solar still utilizing hydrophobic poly (tetrafluoroethylene) nets for separating neighboring wicks, *Desalination* 105 (1996) 207–217, [https://doi.org/10.1016/0011-9164\(96\)00078-1](https://doi.org/10.1016/0011-9164(96)00078-1).
- [14] H. Tanaka, T. Nosoko, T. Nagata, Parametric investigation of a basin-type-multiple-effect coupled solar still, *Desalination* 130 (2000) 295–304, <https://doi.org/10.1016/j.desal.2005.02.046>.
- [15] T. Nosoko, T. Kinjo, C.D. Park, Theoretical analysis of a multiple-effect diffusion still producing highly concentrated seawater, *Desalination* 180 (2005) 33–45, <https://doi.org/10.1016/j.desal.2004.09.031>.
- [16] H. Tanaka, Thermal distillation system utilizing biomass energy burned in stove by means of heat pipe, *Alexandria Eng. J.* 55 (2016) 2203–2208, <https://doi.org/10.1016/j.aej.2016.06.008>.
- [17] C.D. Park, B.J. Lim, K.Y. Chung, Experimental results of a seawater distiller utilizing waste heat of a portable electric generator, *Desalin. Water Treat.* 31 (2011) 134–137, <https://doi.org/10.5004/dwt.2011.2367>.
- [18] C.D. Park, B.J. Lim, K.Y. Chung, Two-effect distillation of a seawater distiller utilizing waste heat of a small electric generator, *Desalin. Water Treat.* 33 (2011) 359–364, <https://doi.org/10.5004/dwt.2011.2668>.
- [19] C.D. Park, B.J. Lim, H. Tanaka, Development of seawater distiller utilizing waste heat of portable electric generators, *Trans. Korean Soc. Mech. Eng. B.* 34 (2010) 607–613, <https://doi.org/10.3795/KSME-B.2010.34.6.607>.
- [20] G. Xie, J. Xiong, H. Liu, B. Xu, H. Zheng, Y. Yang, Experimental and numerical investigation on a novel solar still with vertical ripple surface, *Energy Convers. Manag.* 98 (2015) 151–160, <https://doi.org/10.1016/j.enconman.2015.03.099>.
- [21] K.S. Reddy, H. Sharon, Active multi-effect vertical solar still: mathematical modeling, performance investigation and enviro-economic analyses, *Desalination* 395 (2016) 99–120, <https://doi.org/10.1016/j.desal.2016.05.027>.
- [22] H. Tanaka, T. Nosoko, T. Nagata, Experimental study of basin-type, multiple-effect, diffusion-coupled solar still, *Desalination* 150 (2002) 131–144, [https://doi.org/10.1016/S0011-9164\(02\)00938-4](https://doi.org/10.1016/S0011-9164(02)00938-4).
- [23] H. Tanaka, T. Nosoko, T. Nagata, A highly productive basin-type-multiple-effect coupled solar still, *Desalination* 130 (2000) 279–293, [https://doi.org/10.1016/S0011-9164\(00\)00092-8](https://doi.org/10.1016/S0011-9164(00)00092-8).
- [24] S.D. Yeo, B.J. Lim, G.R. Lee, C.D. Park, Experimental study of effects of different heat sources on the performance of the hybrid multiple-effect diffusion solar still, *Sol. Energy* 193 (2019) 324–334, <https://doi.org/10.1016/j.solener.2019.09.062>.
- [25] C.D. Park, B.J. Lim, K.Y. Chung, S.S. Lee, Y.M. Kim, Experimental evaluation of hybrid solar still using waste heat, *Desalination* 379 (2016) 1–9, <https://doi.org/10.1016/j.desal.2015.10.004>.
- [26] C.D. Park, B.J. Lim, Y.D. Noh, S.S. Lee, K.Y. Chung, Parametric performance test of distiller utilizing solar and waste heat, *Desalin. Water Treat.* 55 (2015) 3303–3309, <https://doi.org/10.1080/19443994.2014.946712>.
- [27] A.K. Kaushal, M.K. Mittal, D. Gangacharyulu, An experimental study of floating wick basin type vertical multiple effect diffusion solar still with waste heat recovery, *Desalination* 414 (2017) 35–45, <https://doi.org/10.1016/j.desal.2017.03.033>.
- [28] H. Tanaka, Y. Nakatake, Outdoor experiments of a vertical diffusion solar still coupled with a flat plate reflector, *Desalination* 214 (2007) 70–82, <https://doi.org/10.1016/j.desal.2006.08.016>.
- [29] H. Tanaka, K. Iishi, Experimental study of a vertical single-effect diffusion solar still coupled with a tilted wick still, *Desalination* 402 (2017) 19–24, <https://doi.org/10.1016/j.desal.2016.09.031>.
- [30] H. Tanaka, Theoretical analysis of a vertical multiple-effect diffusion solar still coupled with a tilted wick still, *Desalination* 377 (2016) 65–72, <https://doi.org/10.1016/j.desal.2015.09.013>.
- [31] B.J. Huang, T.L. Chong, H.S. Chang, P.H. Wu, Y.C. Kao, Solar distillation system based on multiple-effect diffusion type still, *J. Sustain. Dev. Energy, Water Environ. Syst.* 2 (2014) 41–50, <https://doi.org/10.13044/j.sdewes.2014.02.0004>.
- [32] T.L. Chong, B.J. Huang, P.H. Wu, Y.C. Kao, Multiple-effect diffusion solar still coupled with a vacuum-tube collector and heat pipe, *Desalination* 347 (2014)

- 66–76, <https://doi.org/10.1016/j.desal.2014.05.023>.
- [33] L. Huang, H. Jiang, Y. Wang, Z. Ouyang, W. Wang, B. Yang, H. Liu, X. Hu, Enhanced water yield of solar desalination by thermal concentrated multistage distiller, *Desalination* 477 (2020) 114260, <https://doi.org/10.1016/j.desal.2019.114260>.
- [34] K. Fukui, T. Nosoko, H. Tanaka, T. Nagata, A new maritime lifesaving multiple-effect solar still design, *Desalination* 160 (2004) 271–283, [https://doi.org/10.1016/S0011-9164\(04\)90029-X](https://doi.org/10.1016/S0011-9164(04)90029-X).
- [35] B.J. Lim, S.S. Yu, K.Y. Chung, C.D. Park, Numerical analysis of the performance of a tiltable multi-effect solar distiller, *Desalination* 435 (2018) 23–34, <https://doi.org/10.1016/j.desal.2017.12.035>.
- [36] S.A. Kalogirou, Environmental characteristics, *Sol. Energy Eng.*, Elsevier, 2009, pp. 49–762, <https://doi.org/10.1016/B978-0-12-374501-9.00002-9>.
- [37] K.G.T. Hollands, T.E. Unny, G.D. Raithby, L. Konicek, Free convective heat transfer across inclined air layers, *J. Heat Transf.* 98 (1976) 189, <https://doi.org/10.1115/1.3450517>.
- [38] J.P. Holman, *Heat Transfer*, 10th ed., McGraw-Hill, New York, 2009.
- [39] J. Fernández, N. Chargo, Multi-stage, indirectly heated solar still, *Sol. Energy* 44 (1990) 215–223, [https://doi.org/10.1016/0038-092X\(90\)90150-B](https://doi.org/10.1016/0038-092X(90)90150-B).
- [40] M. Garfi, E. Cadena, D. Sanchez-Ramos, I. Ferrer, Life cycle assessment of drinking water: comparing conventional water treatment, reverse osmosis and mineral water in glass and plastic bottles, *J. Clean. Prod.* 137 (2016) 997–1003, <https://doi.org/10.1016/j.jclepro.2016.07.218>.
- [41] A. Livingston, Bottled water vs. tap water – facts & 4 reasons to drink tap, (n.d.). <https://www.moneycrashers.com/bottled-water-vs-tap-water-facts/>.
- [42] How Much Does Bottled Water Cost? <https://www.bottledwater.org/economics/real-cost-of-bottled-water>, (2016).
- [43] D. Carlucci, B. De Gennaro, L. Roselli, What is the value of bottled water? Empirical evidence from the Italian retail market, *Water Resour. Econ.* 15 (2016) 57–66, <https://doi.org/10.1016/j.wre.2016.07.001>.
- [44] H. Tanaka, Y. Nakatake, K. Watanabe, Parametric study on a vertical multiple-effect diffusion-typesolar still coupled with a heat-pipe solar collector, *Desalination* 171 (2005) 243–255, <https://doi.org/10.1016/j.desal.2004.04.006>.
- [45] S.C. Maroo, D.Y. Goswami, Theoretical analysis of a single-stage and two-stage solar driven flash desalination system based on passive vacuum generation, *Desalination* 249 (2009) 635–646 <http://www.sciencedirect.com/science/article/pii/S0011916409008248> accessed February 12, 2014.
- [46] O. Bait, Exergy, environ–economic and economic analyses of a tubular solar water heater assisted solar still, *J. Clean. Prod.* 212 (2019) 630–646, <https://doi.org/10.1016/j.jclepro.2018.12.015>.
- [47] H.E.S. Fath, M. El-Samanoudy, K. Fahmy, A. Hassabou, Thermal-economic analysis and comparison between pyramid-shaped and single-slope solar still configurations, *Desalination* 159 (2003) 69–79, [https://doi.org/10.1016/S0011-9164\(03\)90046-4](https://doi.org/10.1016/S0011-9164(03)90046-4).
- [48] A.A. El-Sebaili, E. El-Bialy, Advanced designs of solar desalination systems: a review, *Renew. Sust. Energ. Rev.* 49 (2015) 1198–1212, <https://doi.org/10.1016/j.rser.2015.04.161>.
- [49] G. Yaciuk, Agricultural applications of solar energy, *Sol. Energy Convers. II*, Elsevier, 1981, pp. 337–353, <https://doi.org/10.1016/B978-0-08-025388-6.50047-7>.